

# An Efficient and Stable Method for Fluid-Rigid Body Interactions with Free Surface

Gwangsoo Go and Hyung Taek Ahn  
Corresponding author : htahn@ulsan.ac.kr

University of Ulsan, Republic of Korea

**Abstract:** In order to simulate fluid-body interaction, many studies have been conducted, and these are generally separated as several types according to its grid system such as body-fitted and Cartesian. When free surface is inserted in fluid-body interaction, three different continuums (air, water, body) should be considered. In this case, Cartesian grid based methodology is most suitable in terms of convenience and efficiency. A robust and efficient method simulating monolithic fluid-rigid body interactions in Cartesian grid was proposed by Gibou and Min [1]. This approach solves the incompressible flow using semi-Lagrangian time discretization with projection method, and strongly couples the fluid and rigid body via projection step by applying fractional time stepping to solid equations. Interestingly, this methodology is proved to be stable in the sense that its kinetic energy does not increase.

We employ this unconditionally stable scheme to simulate fluid-rigid body interaction and combine this method with free surface utilizing volume-of-fluid (VOF) approach. To demonstrate applicability of our numerical method, several benchmark problems are simulated, and all results are validated.

*Keywords:* Fluid-rigid body interaction, semi-Lagrangian time discretization, Projection method, Volume-of-Fluid method.

## 1 Introduction

In many engineering fields, the fluid-rigid body interaction with free surface is the important problems. The ship on the wave and dynamic motion of offshore structures are representative examples of this problem. In this problem, three different continuums, i.e. gas, liquid, and rigid-body, should be simultaneously simulated. Because it is very hard to be solved by applying analytical approach such as potential (ideal flow) theory, the CFD (computational fluid dynamics) simulation should be applied to solve this complex problem.

In the CFD fields, the numerical method can be divided into two types according to its grid system. One is the body-fitted grid[2], and the other is the Cartesian grid[1,3-5]. Although the body-fitted grid system can well resolve the boundary layer so that friction forces are accurately predicted, it has limitation to analyze the moving object. In order to simulate the fluid-body interaction on body-fitted grid, mesh should be deformed or re-generated. On the contrary, the Cartesian grid method can efficiently consider moving body. Furthermore, free surface motion is also efficiently simulated in the Cartesian grid system.

The IBM (immersed boundary method) [3,4] has been successfully applied to analyze the fluid-rigid body interaction in the Cartesian grid system. The fluid and the rigid body are weakly coupled in the standard IBM. Weakly coupling means that the fluid and the rigid-body are separately solved.

Although there are several studies for strongly coupling using iteration scheme, it is very hard to guarantee the stability of the IBM. Once, a robust and efficient method simulating monolithic fluid-body interactions was proposed by Gibou and Min [1]. In this method, both governing equations for the fluid and rigid-body are solved by fractional step method also known as projection method so that the fluid and rigid-body motion are updated to next time step at the same time via projection step. This approach can guarantee numerical stability of fluid-body interaction. However, there is no study yet to combine this stable interaction algorithm with free surface flow.

In this study, the stable fluid-rigid body interaction is combined with free surface flow. In order to compute the dynamic motion of the free surface, the THINC/WLIC (tangent of hyperbola interface capturing/weighted line interface calculation) [6] method is considered. There are several advanced methodology to accurately predict free surface flow such as VOF/PLIC (volume-of-fluid/piecewise linear interface calculation) [7] and MOF (moment-of-fluid) [8]. However, these methods are difficult to implement, especially for three-dimensional case. The THINC/WLIC is easy to implement, but it can effectively simulate free surface flow.

Finally, in order to demonstrate validity of current approach, four different well-known benchmark problems are computed such as flow past a circular cylinder, free falling cylinder, dam-break, and water entry problems. All simulation results are validated with experimental and computational data presented by other researchers.

## 2 Numerical Algorithm

### 2.1 Governing equations for incompressible flow

As governing equations for the fluid, incompressible continuity and Navier-Stokes Equations are defined as

$$\nabla \cdot \mathbf{U} = 0 \quad (1)$$

$$\rho \frac{D\mathbf{U}}{Dt} = -\nabla p + \mu \nabla^2 \mathbf{U} + \rho \mathbf{g} \quad (2)$$

where  $\mathbf{U}$  and  $p$  respectively refer to fluid velocity and pressure as unknowns of governing equations,  $\rho$  is the fluid density,  $\mu$  is the fluid viscosity,  $\mathbf{g}$  means the gravitational acceleration, and  $D/Dt$  means total derivative operator of time

Semi-Lagrangian method is implemented at fixed grid, and departure points( $\mathbf{x}_d^n$ ) of fluid particles arriving at grid points( $\mathbf{x}^{n+1}$ ) are backward tracked along the characteristic lines, i.e.  $D\mathbf{x}/Dt = \mathbf{U}(\mathbf{x}, t)$ . The second-order BDF (backward differentiation formula) is utilized to discretization of left hand side of Eq. (2). Therefore, Eq. (2) can be implicitly discretized in time as follows:

$$\rho \frac{\frac{3}{2}\mathbf{U}^{n+1} - 2\mathbf{U}_d^n + \frac{1}{2}\mathbf{U}_d^{n-1}}{\Delta t} = (-\nabla p + \mu \nabla^2 \mathbf{U} + \rho \mathbf{g})^{n+1}, \quad (3)$$

where variables which has superscript  $n + 1$  is defined at grid points,  $\mathbf{u}_d^n$  and  $\mathbf{u}_d^{n-1}$  are fluid velocities of departure points defined at time  $t^n$  and  $t^{n-1}$ , respectively. Based on RK2 (Runge-Kutta 2) method, a departure point of time  $t^n$  is computed as

$$\mathbf{x}_d^{n+\frac{1}{2}} = \mathbf{x}^{n+1} - \frac{\Delta t}{2} \mathbf{U}^n(\mathbf{x}^{n+1}), \quad (4)$$

$$\mathbf{x}_d^n = \mathbf{x}^{n+1} - \Delta t \mathbf{U}^{n+\frac{1}{2}}\left(\mathbf{x}_d^{n+\frac{1}{2}}\right). \quad (5)$$

Here,  $\mathbf{U}^{n+1/2}$  is estimated by linear extrapolation using the two previous time step, i.e.  $\mathbf{U}^{n+1/2} = 3/2 \mathbf{U}^n - 1/2 \mathbf{U}^{n-1}$ . A departure point of time  $\mathbf{x}_d^{n-1}$  can be similarly determined. Generally, departure point does not coincide with a grid point. In this case, bilinear interpolation is employed to determine the values of departure point.

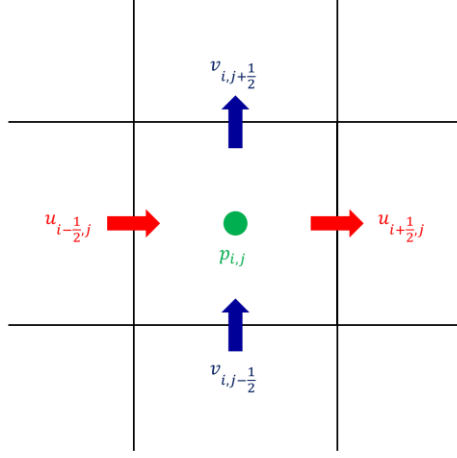


Figure 1: Staggered grid system

In order to solve the implicitly discretized Navier-Stokes equations, standard projection method is employed together with staggered grid system shown in Figure 1. In this grid system, horizontal velocity ( $u_{i\pm 1/2,j}$ ) is positioned at center of vertical plane ( $\mathbf{x}_{i\pm 1/2,j}$ ), vertical velocity ( $v_{i,j\pm 1/2}$ ) is located at center of horizontal plane ( $\mathbf{x}_{i,j\pm 1/2}$ ), and pressure ( $p_{i,j}$ ) is defined at center of grid ( $\mathbf{x}_{i,j}$ ). This grid system has an advantage to effectively satisfy the incompressibility.

## 2.2 Governing equations for rigid-body

The dynamic motion of rigid-body interacted with the fluid is described by

$$\frac{d\mathbf{P}}{dt} = m\mathbf{g} + \oint (-p\mathbf{I} + 2\mu\mathbf{D}) \cdot \mathbf{n} d\Gamma, \quad (6)$$

$$\frac{d\mathbf{L}}{dt} = \oint \mathbf{r} \times (-p\mathbf{I} + 2\mu\mathbf{D}) \cdot \mathbf{n} d\Gamma, \quad (7)$$

where  $m$  is the mass of the rigid body,  $\mathbf{P}$  and  $\mathbf{L}$  represent respectively linear momentum and angular momentum of rigid-body,  $\mathbf{g}$  means gravitational acceleration,  $\mathbf{n}$  refer to outward-positive surface normal vector of rigid-body,  $\Gamma$  is the interface between fluid and rigid-body,  $\mathbf{r}$  is the position vector whose origin is the center of rigid-body,  $\mathbf{I}$  is identity tensor, and  $\mathbf{D}$  is the strain rate tensor of fluid velocity that is defined as

$$\mathbf{D} = \frac{1}{2} \left( \frac{\partial U_i}{\partial x_j} + \frac{\partial U_j}{\partial x_i} \right). \quad (8)$$

Using computed  $\mathbf{P}$  and  $\mathbf{L}$ , the location of body's center of mass  $\mathbf{C}$  and the orientation matrix  $\mathbf{R}$  of the rigid-body can be determined as

$$\frac{d\mathbf{C}}{dt} = \frac{\mathbf{P}}{m} \quad \text{and} \quad \frac{d\mathbf{R}}{dt} = \boldsymbol{\omega} \times \mathbf{R}, \quad (9)$$

where  $\boldsymbol{\omega} = \mathbf{I}^{-1}\mathbf{L}$  is the angular velocity of the rigid-body.  $\mathbf{I}$  means the inertia matrix of the rigid-body.

## 2.3 Fluid-rigid body interaction

### 2.3.1 Heaviside function

In order to efficiently treat irregular fluid domain induced by the rigid-body, the Heaviside function  $H$  which is 0 at the body region and 1 at the solid region is employed. Using relation for  $\nabla H = \mathbf{n}\delta_f$ , the projection method that can be considered at following subsection can be robustly applied in the entire domain. Furthermore, the fluid forces and moments acting on the rigid-body also simply computed in the entire domain. In finite volume approach, Heaviside function is defined as length fraction at two-spatial dimension and area fraction at three-spatial dimension.

In the case of two-spatial dimension, the Heaviside function at vertical surface is defined as

$$H_{i+\frac{1}{2},j} = \frac{\phi_{i+\frac{1}{2},j+\frac{1}{2}}^+ - \phi_{i+\frac{1}{2},j-\frac{1}{2}}^+}{\phi_{i+\frac{1}{2},j+\frac{1}{2}} - \phi_{i+\frac{1}{2},j-\frac{1}{2}}} \quad (10)$$

where  $\phi$  means signed distance function of rigid-body, and  $\phi^+ = \max(\phi, 0)$ . If both  $\phi_{i+1/2,j+1/2}$  and  $\phi_{i+1/2,j-1/2}$  are positive, the Heaviside function is 1. On the contrary, if both are negative, then the Heaviside function is 0. Similarly, the Heaviside function at horizontal surface can be computed.

In the case of three-spatial dimension, the Heaviside function is defined as the sum of area fraction of two triangles composing the rectangular surface. If  $\phi_0, \phi_1, \phi_2, \phi_3$  are considered as signed distance function at four grid points of the cell surface, the area fraction of triangle  $\Delta P_0 P_1 P_2$  is computed as

$$H(\phi_0, \phi_1, \phi_2) = \begin{cases} \frac{\phi_0^+ - \phi_1^+}{\phi_0 - \phi_1} \cdot \frac{\phi_0^+ - \phi_2^+}{\phi_0 - \phi_2} & \text{if } \phi_0 > 0, \phi_1 < 0, \text{ and } \phi_2 < 0, \\ 1 - \frac{\phi_0^- - \phi_1^-}{\phi_0 - \phi_1} \cdot \frac{\phi_0^- - \phi_2^-}{\phi_0 - \phi_2} & \text{if } \phi_0 < 0, \phi_1 > 0, \text{ and } \phi_2 > 0, \end{cases} \quad (11)$$

where  $\phi^- = \min(\phi, 0)$ . Similarly, the area fraction of other triangle  $\Delta P_0 P_3 P_2$  can be calculated. Finally, the Heaviside function of rectangular surface is defined as

$$H(\phi_0, \phi_1, \phi_2, \phi_3) = \frac{1}{2} (H(\phi_0, \phi_1, \phi_2) + H(\phi_0, \phi_3, \phi_2)). \quad (12)$$

The aforementioned discretization of the Heaviside function in two-spatial dimension produces about 1.5 order of accuracy. However, discretization in three-spatial dimension has second order of accuracy.

### 2.3.2 Projection method for fluid

The incompressible Navier-Stokes equations are solved by the standard projection method [9]. In the projection method, the single time evolution is divided into two stages, i.e. intermediate state and projection step.

Firstly, intermediate state(\*) of semi-Lagrangian Navier-Stokes equation is given by

$$\rho \frac{\frac{3}{2} \mathbf{U}^* - 2\mathbf{U}_d^n + \frac{1}{2} \mathbf{U}_d^{n-1}}{\Delta t} = \mu \nabla^2 \mathbf{U}^* + \rho \mathbf{g}^{n+1}, \quad (13)$$

where  $\mathbf{U}^* = \mathbf{U}_{body}^{n+1}$  at body surface. The fluid velocity at intermediate state  $\mathbf{U}^*$  cannot satisfy the incompressibility ( $\nabla \cdot \mathbf{U} = 0$ ), thus it has no physical meaning. The equations of intermediate state can be defined to velocity Poisson equation. In order to efficiently solve the this Poisson equation with satisfying no-slip boundary condition at body surface, a second-order accurate discretization method

of Poisson equation on irregular domain proposed by Gibou et al.[10] is applied. Because this method produces symmetric positive definite system, the conjugate gradient method is applied as appropriate solver.

Following projection step is

$$\mathbf{U}^{n+1} = \mathbf{U}^* - \frac{\Delta t}{\rho} \nabla q^{n+1}, \quad (14)$$

where  $q$  is the scalar quantity to enforce the incompressibility of the fluid. If Eq.(14) is substituted into Eq.(13), it should be same as original Navier-Stokes equation Eq.(3). Using this relation, the pressure can be calculated by

$$p^{n+1} = \frac{3}{2} q^{n+1} - \mu \nabla \cdot \mathbf{U}^*. \quad (15)$$

The scalar quantity  $q$  is determined by Poisson equation that will be described in following sub-section 2.3.4.

### 2.3.3 Projection method for rigid-body

The governing equations for the rigid-body are also solved by fractional step method. As mentioned in previous sub-section, the single time evolution is divided into two step, i.e. intermediate state and projection step. The reason why this fractional time stepping can be applied to the rigid-body equation is that the projection step of the rigid body satisfies Hodge decomposition (the vector field can be uniquely decomposed into a divergence-free and an irrotational part).

The intermediate state of governing equations of the rigid body is

$$\frac{\frac{3}{2} \mathbf{P}^* - 2\mathbf{P}^n + \frac{1}{2} \mathbf{P}^{n-1}}{\Delta t} = 2\mathbf{f}_v^n - \mathbf{f}_v^n + \rho \mathbf{g}^{n+1}, \quad (16)$$

$$\frac{\frac{3}{2} \mathbf{L}^* - 2\mathbf{L}^n + \frac{1}{2} \mathbf{L}^{n-1}}{\Delta t} = 2\boldsymbol{\tau}_v^n - \boldsymbol{\tau}_v^{n-1}, \quad (17)$$

where  $\mathbf{f}_v = \int (2\mu \mathbf{D}) \cdot \mathbf{n} d\Gamma$  and  $\boldsymbol{\tau}_v = \int \mathbf{r} \times (2\mu \mathbf{D}) \cdot \mathbf{n} d\Gamma$ . Using the linear extrapolation,  $\mathbf{f}_v^{n+1}$  and  $\boldsymbol{\tau}_v^{n+1}$  are approximated by  $2\mathbf{f}_v^n - \mathbf{f}_v^n$  and  $2\boldsymbol{\tau}_v^n - \boldsymbol{\tau}_v^{n-1}$ , respectively. Because the linear and angular momentum at intermediate state are updated by only viscous forces and moments of the fluid, they have no physical meaning.

The following projection step is

$$\mathbf{P}^{n+1} = \mathbf{P}^* - \Delta t \oint_{\Gamma} q^{n+1} \mathbf{n} d\Gamma = \mathbf{P}^* - \Delta t \int_{\Omega} q^{n+1} \nabla H^{n+1} d\Omega, \quad (18)$$

$$\mathbf{L}^{n+1} = \mathbf{L}^* - \Delta t \oint_{\Gamma} \mathbf{r} \times q^{n+1} \mathbf{n} d\Gamma = \mathbf{L}^* - \Delta t \int_{\Omega} \mathbf{r} \times q^{n+1} \nabla H^{n+1} d\Omega. \quad (19)$$

As described in section 2.3.1,  $\nabla H = \mathbf{n} \delta_r$  so that the surface integral can be simply computed in entire domain.

### 2.3.4 Poisson equation for scalar quantity $q$

If the scalar quantity  $q$  is determined, governing equations for the fluid and the rigid-body are simultaneously solved without any numerical coupling method. It means that the fluid and the rigid-

body are monolithically interacted. This strongly coupled interaction algorithm is proved to be stable in the sense that its kinetic energy does not increase by Gibou and Min [1].

Based on incompressibility of the fluid and non-penetration condition at body surface, the Poisson equation for  $q$  is derived by

$$\nabla \cdot \left( H^{n+1} (\mathbf{U}^{n+1} - \mathbf{U}_{body}^{n+1}) \right) = \nabla \cdot (H^{n+1} \mathbf{U}^{n+1}) - \nabla H^{n+1} \cdot \mathbf{U}_{body}^{n+1} = 0. \quad (20)$$

Substituting Eqs. (14) and (18)-(19) into Eq.(20), the Poisson equation for  $q$  is defined as

$$\begin{aligned} & -\nabla \cdot \left( \frac{H^{n+1}}{\rho} \nabla q^{n+1} \right) + \nabla H^{n+1} \cdot \frac{1}{m} \left( \int_{\Omega} q^{n+1} \nabla H^{n+1} d\Omega \right) + \mathbf{J}^{n+1} \cdot ((I^{-1})^{n+1}) \left( \int_{\Omega} q^{n+1} \mathbf{J}^{n+1} d\Omega \right) \\ & = -\frac{1}{\Delta t} \nabla \cdot (H^{n+1} \mathbf{U}^*) + \frac{1}{\Delta t} \nabla H^{n+1} \cdot \mathbf{U}_{body}^*, \end{aligned} \quad (21)$$

where

$$\mathbf{J}^{n+1} = \mathbf{r} \times \nabla H^{n+1} \quad \text{and} \quad \mathbf{U}_{body}^* = \frac{\mathbf{P}^*}{m} + ((I^{-1})^{n+1} \mathbf{L}^*) \times \mathbf{r}. \quad (22)$$

Although the Poisson equation for  $q$  produces symmetric positive definite system, the geometric Multigrid solver is applied to solve this Poisson equation. We believe that the geometric Solver is the most fast solution method for the linear system.

## 2.4 Free surface simulation

### 2.4.1 THINC/WLIC method

The VOF (volume-of-fluid) method is the most preferred approach to simulate multiphase flow due to the mass conservation. The characteristic of fluid is distinguished by characteristic function,  $\chi$ , in the VOF method. The characteristic function is 0 at the gas and 1 at the liquid. In finite volume approach, the volume-averaged value should be needed, thus volume fraction function,  $f$ , is considered and its value is 0 at the gas region, 1 at the liquid region, and between 0 and 1 at the interface region.

In order to satisfy the mass conservation of the fluid, the characteristic function should satisfy

$$\frac{Df}{Dt} = \frac{\partial f}{\partial t} + \nabla \cdot (\mathbf{U}\chi) - \chi \nabla \cdot \mathbf{U} = 0, \quad (23)$$

where  $\mathbf{U}$  is the velocity vector of the fluid.

Based on a dimensional splitting algorithm, volume fraction function  $f$  is updated in time as follows:

$$f_{i,j}^* = f_{i,j}^n - \frac{F_{x,i+1/2,j}^n - F_{x,i-1/2,j}^n}{\Delta x} - f_{i,j}^n \frac{U_{x,i+1/2,j}^n - U_{x,i-1/2,j}^n}{\Delta x} \Delta t, \quad (24)$$

$$f_{i,j}^{n+1} = f_{i,j}^* - \frac{F_{y,i,j+1/2}^n - F_{y,i,j-1/2}^n}{\Delta y} - f_{i,j}^* \frac{U_{y,i+1/2,j}^n - U_{y,i-1/2,j}^n}{\Delta y} \Delta t, \quad (25)$$

where  $F_{x,i+1/2,j}$  and  $F_{y,i,j+1/2}$  are the fluxes of characteristic function about  $x$ - and  $y$ -direction, respectively. There are many studies to accurately compute the flux of characteristic fraction function. Among these methods, we employ the THINC/WLIC (tangent of hyperbola for interface capturing / weighted line interface calculation) method in order to efficiently simulate the free surface flow.

The original VOF method uses Heaviside step function to express the characteristic function of the each cell. However, the smoothed Heaviside function is utilized in the THINC method. Due to smoothed variation of characteristic function, THINC method is known for effectively preventing the

flotsam. By using hyperbolic tangent function, the characteristic function,  $\chi$ , of the one-dimensional THINC scheme is defined as

$$\chi_{x,i} = \frac{1}{2} \left( 1 + \alpha_x \tanh \left( \beta \left( \frac{x - x_{i-1/2}}{\Delta x} - \tilde{x}_i \right) \right) \right), \quad (26)$$

where  $\alpha_x$  and  $\beta$  mean the interface direction and smoothing of the characteristic function, respectively.  $\tilde{x}\Delta x$  is same as the distance between  $x_{i-1/2}$  and the interface.

The WLIC scheme is based on similar interface reconstruction manner like the SLIC (simple line interface calculation) method. In SLIC method [11], vertical and horizontal interfaces are respectively considered for calculating  $x$ - and  $y$ -directional fluxes in two-spatial dimension. However, both vertical and horizontal interfaces are used to compute fluxes of each direction in the WLIC method. Instead, a weight is given for the direction. This weight  $\omega$  is computed using surface normal vector  $\mathbf{n}$ . Therefore, two-dimensional characteristic function can be defined as

$$\chi_{i,j} = \omega_{x,i,j}(\mathbf{n}_{i,j})\chi_{x,i,j} + \omega_{y,i,j}(\mathbf{n}_{i,j})\chi_{y,i,j}. \quad (27)$$

The fluxes can be determined by integration of characteristic function. The details are described in [6].

#### 2.4.2 Numerical test : Reversible S-shape flow

The character  $S$ -shape flow presented in Ahn and Shashkov [8] is considered to validate THINC/WLIC method. The divergence free nonlinear velocity field

$$\mathbf{v} = \left( \frac{1}{4}((4x - 2) + (4y - 2)^3), -\frac{1}{4}((4y - 2) + (4x - 2)^3) \right) \quad (28)$$

changes a circular region into a character  $S$ -shape. After  $S$ -shape is completed, reversible velocity field is applied to return to the original circular shape. Then, the volume fraction of the recovered region is compared to the volume fraction of the original one in order to validate THINC/WLIC method.

The computational domain  $[0,1]^2$  is considered, and the circle whose radius is 0.25 is located at (0.5,0.5). Three different grid levels, i.e. coarse( $100 \times 100$ ), medium( $200 \times 200$ ), fine( $400 \times 400$ ), are used to computation. At time = 3.0s, the character  $S$ -shape is completed. Therefore, velocity field  $\mathbf{v}$  is applied until time=3.0s, then reversible velocity field  $-\mathbf{v}$  is employed.

Figure 2 depicts the time series of snapshots for reversible  $S$ -shape flow. Convergence of the volume differences between original- and recovered region is shown in Table 00. It is confirmed that the THINC/WLIC method produces first-order accurate results based on  $L1$ -error. In this analysis,  $L1$ -error is defined as

$$L1 \text{ error} = \frac{\sum_{i,j} |f_{i,j}^{original} - f_{i,j}^{recovered}|}{\text{number of cells}}. \quad (29)$$

Table 1: Convergence of the volume differences between original- and recovered region

Grid	$L1$ -Error	Order
100x100	0.007412	-
200x200	0.003153	1.23
400x400	0.001567	1.01

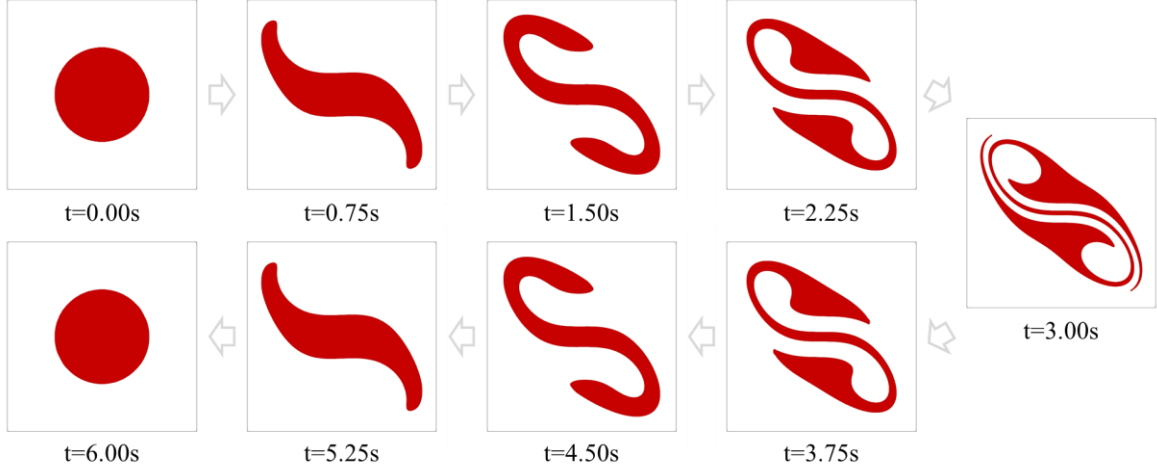


Figure 2: Snapshots of reversible S-shape flow in the case of uniform  $400 \times 400$  mesh

### 3 Simulation results

To demonstrate validity of our numerical method, several benchmark problems are simulated in this section. Firstly, flow past a circular cylinder is computed to validate fluid-body coupling. Secondly, falling cylinder problem is solved to confirm the validity of algorithm of fluid-body interaction. Thirdly, dam-break problem is analyzed to validate violent motion of free surface. Finally, water entry of circular cylinder is computed to demonstrate validity of fluid-body interaction with free surface.

#### 3.1 Fluid-body coupling : Flow past a circular cylinder

The computational domain of flow past a circular cylinder problem is set as shown in Figure 3. Total domain size is considered as  $[-8, 24] \times [-8, 8]$ , and a center of circular cylinder which has radius of 0.5 is located at  $(0,0)$ . We impose Dirichlet boundary condition of  $u = U_\infty = 1$  at the left, the slip boundary condition at top and bottom, the convective boundary condition (convection velocity is average value of right boundary) at the right, and non-slip wall boundary condition at the cylinder's boundary. A  $1024 \times 512$  Cartesian mesh is used in the entire computational domain to well resolve the cylinder body. Because semi-Lagrangian based fluid solver can employ large time step, CFL number ( $U_\infty \Delta t / \Delta x$ ) is set to 4 in this computation. The fluid density is considered as 1, and the viscosity is set with respect to Reynolds number.

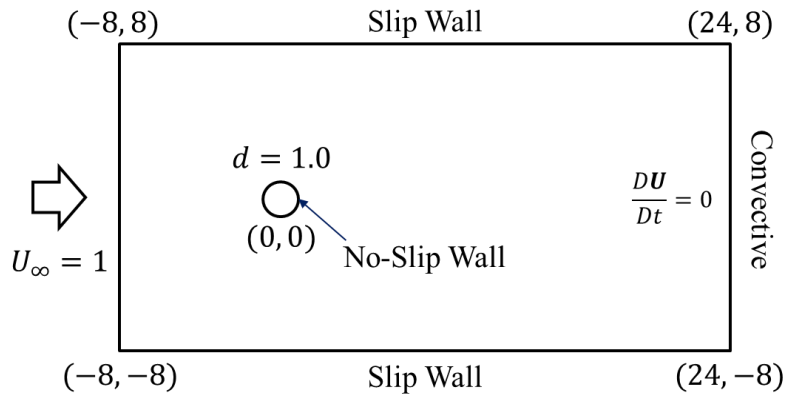


Figure 3: Layout of 2D flow past a circular cylinder problem

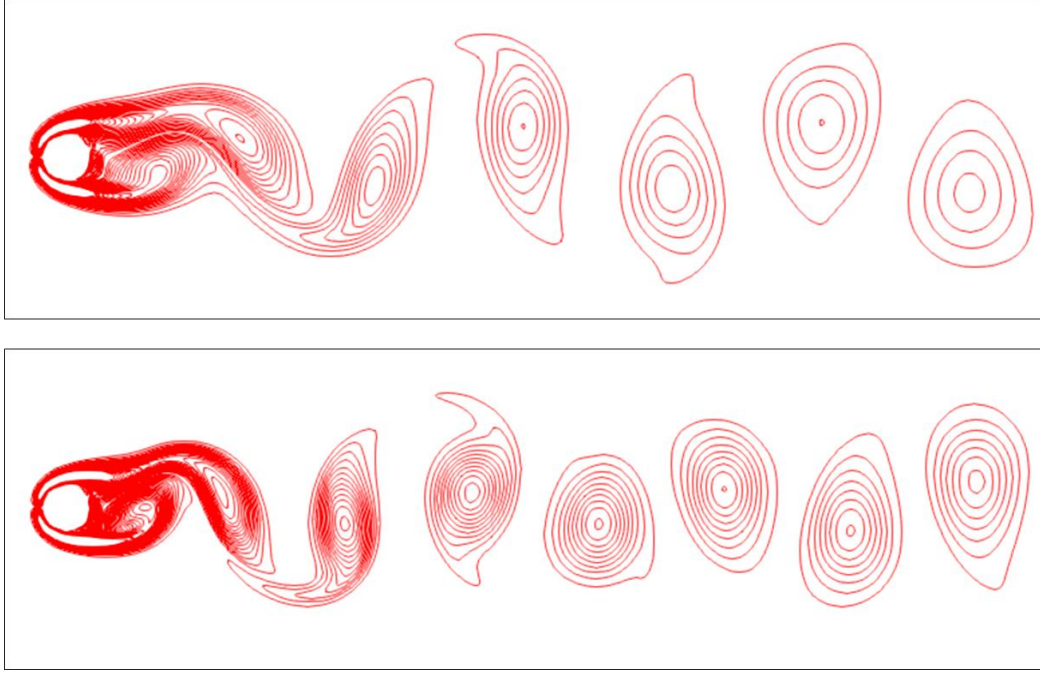


Figure 4: Vorticity contours for  $Re = 100$ (top) and  $200$ (bottom). The size of captured domain is  $[-1,18] \times [-3 \times 3]$ . Contours are presented from  $-4$  to  $4$  with  $41$  intervals.

In order to validate our numerical solution, simulation results are compared with experimental or numerical results presented by other researchers.

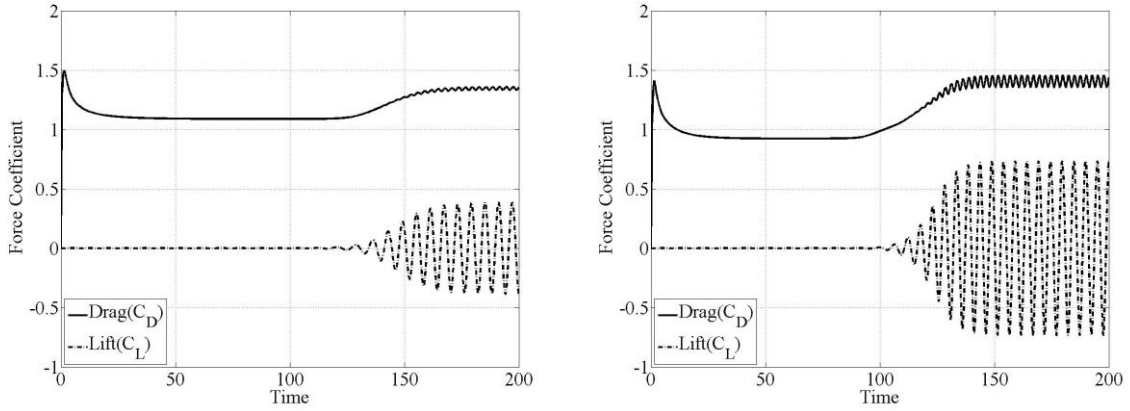


Figure 5: Time history of drag and lift coefficient. Left is for  $Re = 100$ , and Right is for  $Re = 200$ . The solid line refers to drag coefficient, and dotted line indicates lift coefficient.

Firstly, drag and lift coefficients at  $Re = 100, 200$  is compared with both experimental and numerical results. The drag and lift coefficients are defined as

$$C_D = \frac{F_x}{0.5\rho U_\infty^2 d} \text{ and } C_L = \frac{F_y}{0.5\rho U_\infty^2 d}, \quad (30)$$

where  $F_x$  is drag force,  $F_y$  is lift force, and  $d$  means diameter of circular cylinder. In our simulation condition,  $C_D$  and  $C_L$  is simply defined as  $2F_x$  and  $2F_y$ , respectively. Figure 5 shows the time history of drag and lift coefficient, and Table 2 presents unsteady drag and lift coefficients of current study and other studies. As shown in Table 2, our numerical results are in good agreement with other studies.

Table 2: Drag and lift coefficients of current results and other researcher`s results

	$Re = 100$		$Re = 200$	
	$C_D$	$C_L$	$C_D$	$C_L$
Choi et al [3]	$1.34 \pm 0.011$	$\pm 0.315$	$1.36 \pm 0.048$	$\pm 0.64$
Ng et al [5]	$1.37 \pm 0.016$	$\pm 0.36$	$1.37 \pm 0.050$	$\pm 0.72$
Braza et al [12]	$1.36 \pm 0.015$	$\pm 0.25$	$1.40 \pm 0.050$	$\pm 0.75$
Liu et al [13]	$1.35 \pm 0.012$	$\pm 0.339$	$1.31 \pm 0.049$	$\pm 0.69$
<b>Present</b>	$1.34 \pm 0.012$	$\pm 0.37$	$1.40 \pm 0.050$	$\pm 0.73$

Secondly, the Strauhal number ( $St$ ) is compared at low Reynolds number ( $< 200$ ). The Strauhal number is important parameter in designing cable such as deep-sea riser since Strauhal number is directly related with vortex induced vibration. The Strauhal number is defined as

$$St = \frac{fd}{U_\infty}, \quad (31)$$

where  $f$  is shedding frequency which is same as frequency of lift oscillation. In order to compare Strauhal number, additional simulation is conducted at  $Re = 120, 140, 150, 160, 180$ .

Figure 6 shows that our results are well-matched to results of other studies.

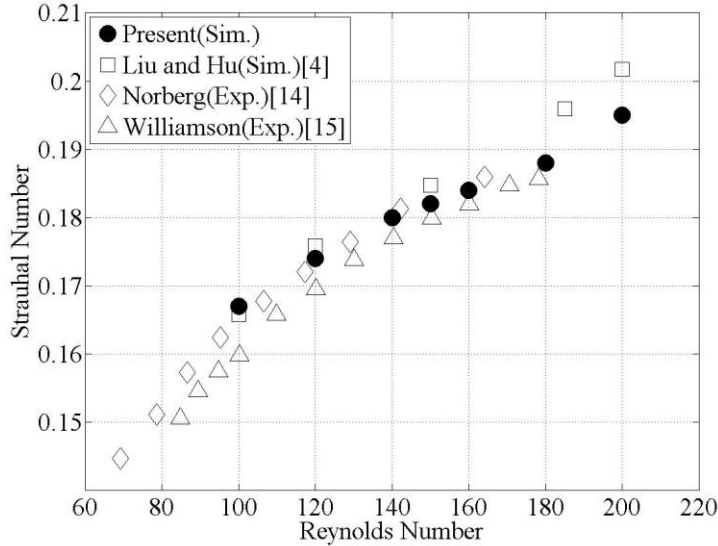


Figure 6: Comparison results of Strauhal number versus Reynolds number

### 3.2 Fluid-body interaction : Falling cylinder problem

To validate numerical algorithm of fluid-rigid body interaction in single phase flow, falling cylinder problem is computed in this section. The size of computational domain is  $[-L, L] \times [0, 8L]$ , and a center of circular cylinder which has radius,  $r$ , of  $0.25L$  is located at  $(0, 6.5L)$ . We impose convective boundary condition at top, and no-slip boundary condition at other boundaries. The length parameter  $L$  is set to  $2 \times 10^{-2}m$ , gravitational acceleration  $g$  is  $9.8m/s$ , fluid`s density,  $\rho_f$ , is  $1 \times 10^3 kg/m^3$ , and cylinder`s density,  $\rho_s$ , is  $2 \times 10^3 kg/m^3$ . An analytical solution [16] of the terminal falling velocity,  $V$ , can be derived utilizing the Stokes assumption of low Reynolds number :

$$V = \frac{(\rho_s - \rho_f)gr^2}{4\mu} \left\{ -\ln\left(\frac{r}{L}\right) - 0.9157 + 1.7244\left(\frac{r}{L}\right)^2 - 1.7302\left(\frac{r}{L}\right)^4 \right\}, \quad (32)$$

where  $\mu$  is fluid's viscosity. Because the validity of Stokes assumption is confirmed at very low Reynold number ( $< 0.1$ ), we take  $\mu = 0.5\text{kg/s}$ . The  $128 \times 512$  Cartesian grid is utilized, and Figures 0-0 depict simulation results. Figure 7 shows snapshots of velocity magnitude contour and streamlines with respect to time. Figure 8 presents comparison results between current simulation and analytical solution. As shown in Figure 8, simulation results are well matched to analytical solution.

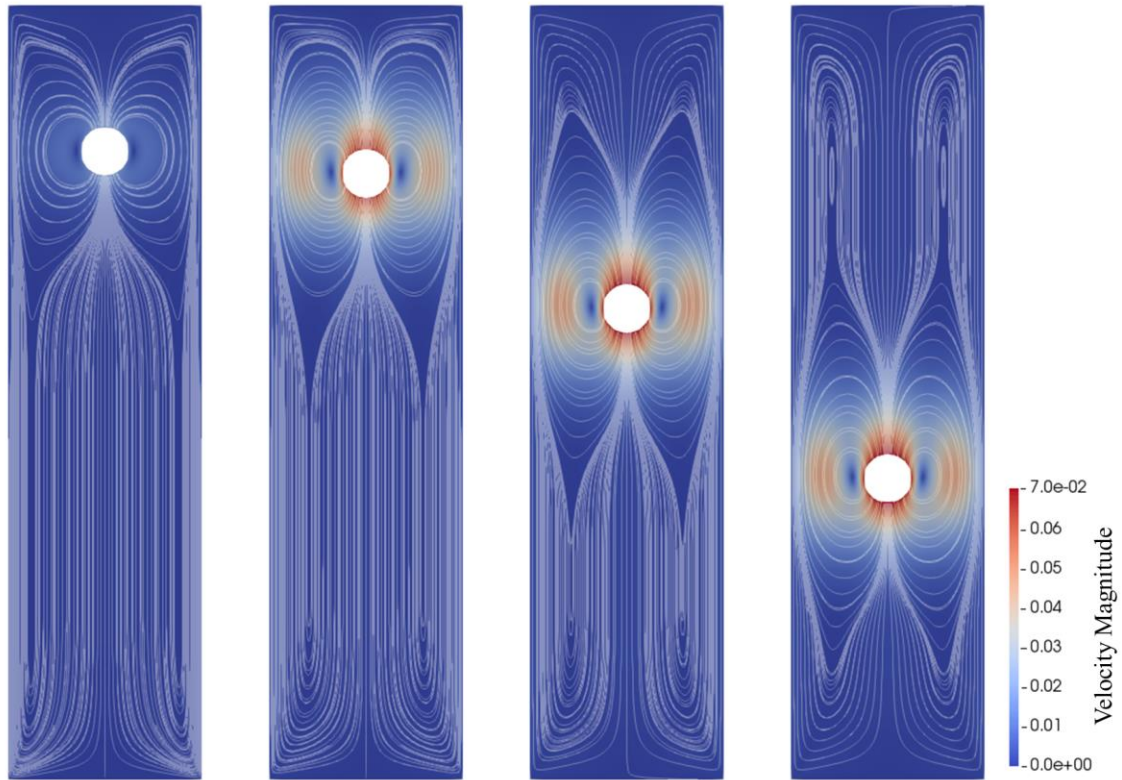


Figure 7: Velocity magnitude contours and streamlines around the falling cylinder with respect to time. From the left,  $t = 0.0\text{s}$ ,  $0.1\text{s}$ ,  $0.5\text{s}$ ,  $1.0\text{s}$ .

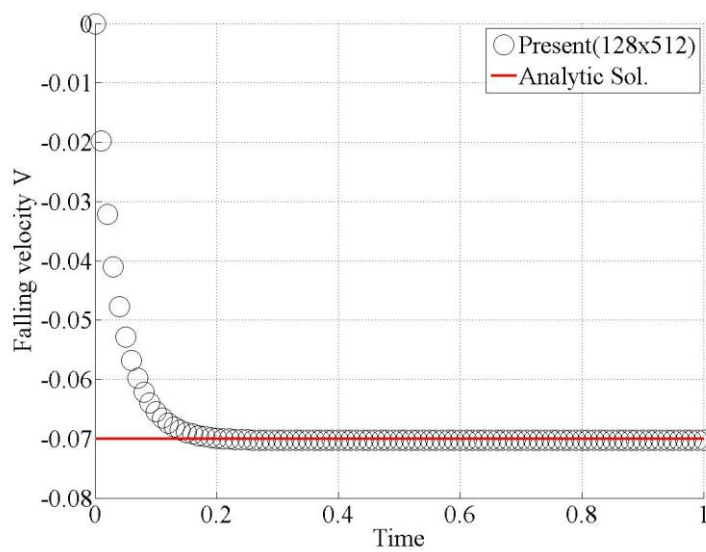


Figure 8: The variation of Falling velocity  $V$  with respect to time. Circle means present simulation, and solid line refers to analytical solution based on Eq. (32).

### 3.3 Free surface flow : Dam-break problem

In order to demonstrate unsteady motion of free surface flow, classical free surface problem, namely dam-break, is computed. In this simulation, liquid and gas is considered as water and air, respectively. The size of computational domain is  $[0, 5a] \times [0, 1.25a]$ , and the configuration of water dam is initially set to  $[0, a] \times [0, a]$ . We take length parameter  $a$  as  $0.05715m$ . All boundaries conditions are imposed as no-slip wall. In the dam-break problem, the density difference, which is about 1000 times, between water and air under gravitational acceleration causes the water to collapse and water to spread into the air. The dam-break problem is computed with different grid level such as coarse( $128 \times 32$ ), medium( $256 \times 64$ ), and fine( $512 \times 128$ ).

Snapshots taken at three different non-dimensional time  $T(= t\sqrt{g/a})$  of breaking procedure are presented as shown in Figure 9. The surge front position,  $S$ , and column height parameter,  $H$ , is employed to be compared with experimental data. These parameters are defined as

$$S = \frac{x(t)}{a} \quad \text{and} \quad H = \frac{y(t)}{a}, \quad (33)$$

where  $x(t)$  is maximum  $x$ -directional displacement of water configuration at bottom wall, and  $y(t)$  is maximum  $y$ -directional displacement of water configuration at left wall. For your better understand, Figure 10 is presented.

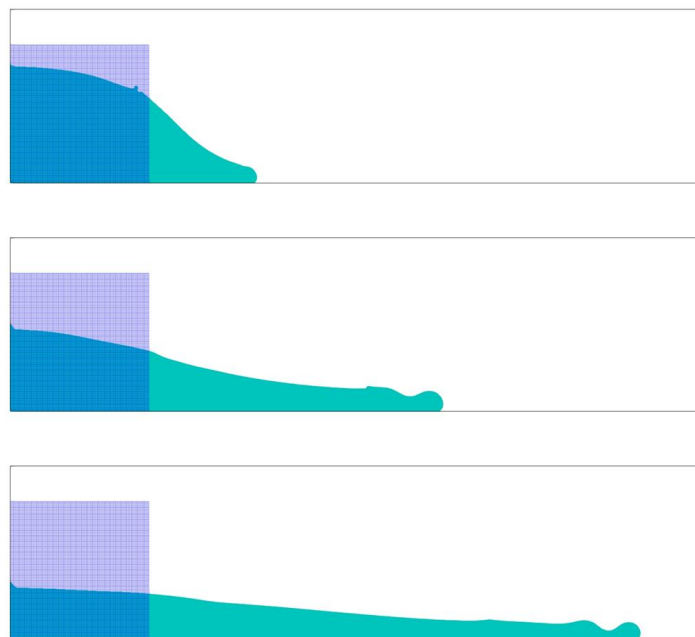


Figure 9: Snapshots of dam-break procedure. Snapshots are taken at non-dimensional time  $T=1.0$ (top),  $2.0$ (middle),  $3$ (bottom). Mesh lines mean initial configuration of water dam.

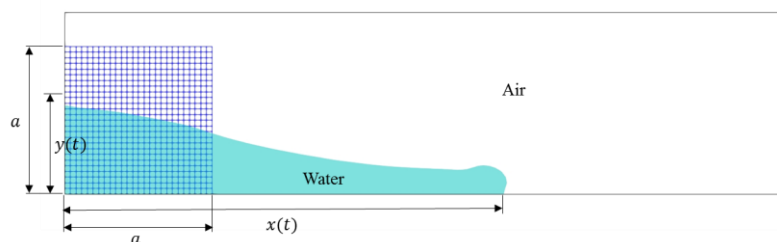


Figure 10: Definition of  $(t)$ ,  $y(t)$ , and  $a$ . The initial configuration of the water dam is indicated by the mesh lines

The variation of surge front position and column height versus non-dimensional time is compared with experimental data. As shown in Figure 11, our simulation results are in good agreement with experimental data [17].

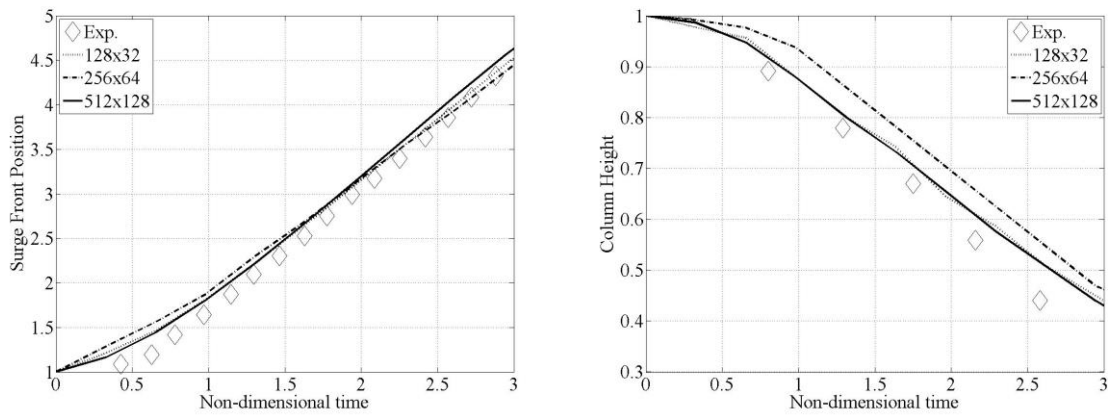


Figure 11: Comparison of surge front position (left) and column height (right) with experimental data

### 3.4 Fluid-body interaction with free surface : Water entry problem

The problem that the rigid body enters into the free surface is known as the water entry problem. The water entry problem is typical benchmark test that can validate algorithm for simulating fluid-body interaction with free surface. In our water entry test, a rigid circular cylinder is initially positioned at air region, and then it freely falls to free surface due to gravity. If the density of the body is smaller than fluid's density, the body floats at free surface. Since the terminal vertical position and falling velocity can be analytically computed by hydrostatics, simulation results of these two parameters are compared with analytical solution.

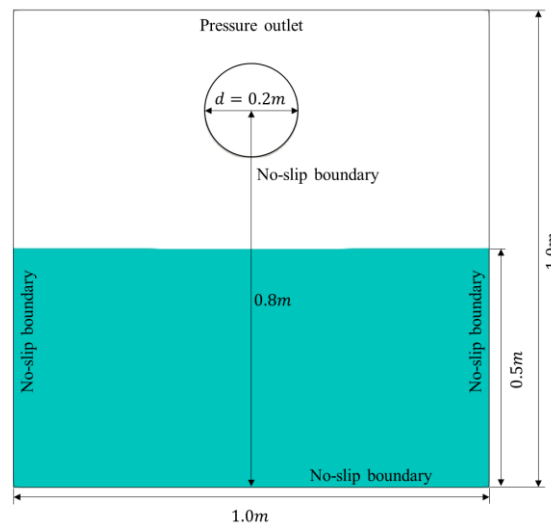


Figure 12: Computational set up of water entry problem

The computational set up of water entry problem is shown in Figure 12. A computational domain of  $[0,1] \times [0,1]$  is considered. The diameter of circular cylinder is  $0.2m$ , and the density of cylinder is set to half of fluid's density. The cylinder is positioned at  $0.8m$  from the bottom, and free surface is located at  $0.5m$  from the bottom. Pressure outlet boundary condition is imposed to top boundary, and all other boundaries are considered as no-slip wall. Gravitational acceleration is  $9.8m/s$ . The  $128 \times 128$  Cartesian mesh is used in this simulation.

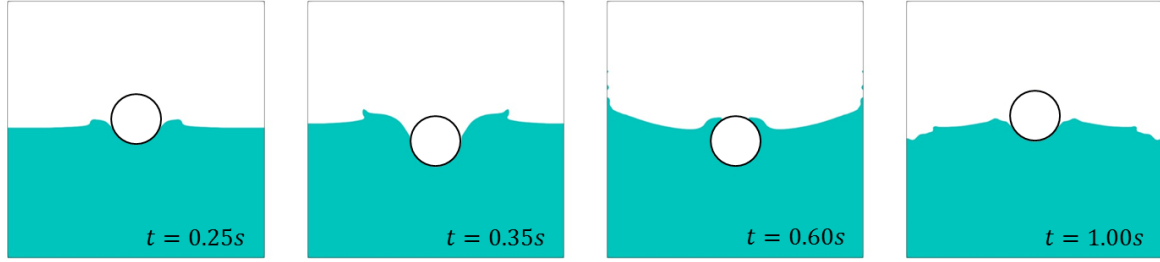


Figure 13: Snapshots of violent motion of free surface during water entry

Figure 13 shows snapshots of violent motion of free surface while cylinder enters into the free surface. The variation of free surface shown in snapshots is in good agreement with physical plausibility. The analytical terminal vertical position of center of cylinder is  $0.5157m$  from the bottom since body's density is set to half of fluid's density in this simulation. Of course, the analytical terminal falling velocity is  $0m/s$ . As shown in Figure 14, simulation results of vertical position and falling velocity are converged to analytical terminal values.

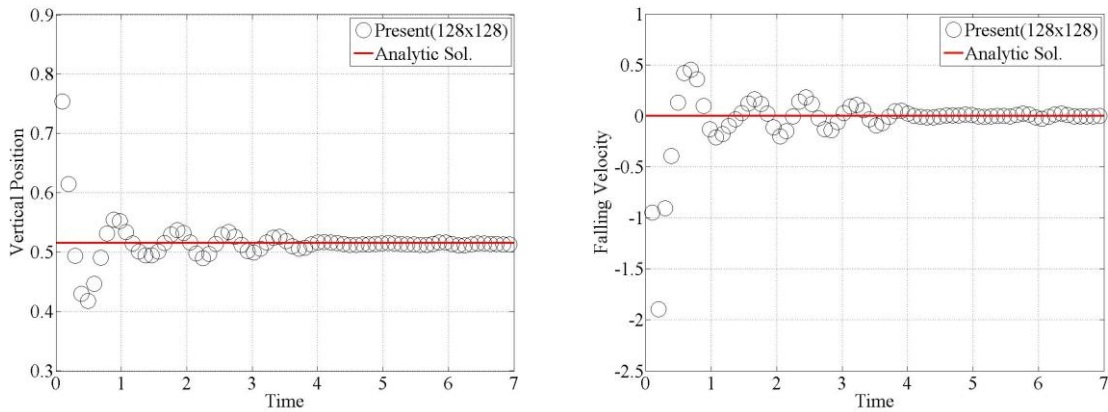


Figure 14: Time history of vertical position and falling velocity of the cylinder. Circle means present simulation, and solid line refers to analytic solution of each terminal values.

## 4 Conclusion and Future Work

The efficient and stable method for monolithic fluid-rigid body interactions with free surface flow was presented in this study. The governing equations for fluid, namely incompressible Navier-Stokes equations, are solved by the implicit semi-Lagrangian time discretization and standard projection method together with Cartesian mesh. The dynamic equations for the rigid-body are also solved by fractional step method. The fluid-rigid body interactions are enforced via projection step so that each equation for the fluid and the rigid-body is simultaneously solved with same time evolution.

The dynamic motion of free surface flow is efficiently simulated by the THINC/WLIC method. Unlike the original VOF method that uses Heaviside step function, THINC scheme utilizes smoothed Heaviside function so that it could effectively prevent flotsam. The WLIC method is based on similar interface reconstruction manner like the SLIC method. However, the WLIC method is superior to the SLIC method by using weighting function with respect to direction.

To demonstrate validity of current approach, four different benchmark problems were computed such as flow past a circular cylinder, free falling cylinder, dam-break, and water entry problems. Based on simulation results of these problems, it is confirmed that three different continuums, i.e. air, water, rigid-body, can be stably and efficiently simulated at the same time with present algorithm.

Because the THINC/WLIC method produces first-order accurate results, the more advanced method will be need. For this reason, combination of present stable fluid-rigid body interaction algorithm and the MOF (moment-of-fluid) method is considered as primary research in the future.

## 5 Acknowledgement

This work was supported by National Research Foundation of Korea (NRF) Grant funded by the Korean Government (NRF-2017-Global Ph.D Fellowship Program).

## References

- [1] F. Gibou and C. Min. Efficient symmetric positive definite second-order accurate monolithic solver for fluid/solid interactions. *J. Comput. Phys.*, 231:3246-3263, 2012.
- [2] H. T. Ahn and Y. Kallinderis. Strongly coupled flow/structure interactions with a geometrically conservative ALE scheme on general hybrid meshes. *J. Comput. Phys.*, 219:671-696, 2006.
- [3] J. I. Choi, R. C. Oberoi, J. R. Edwards, and J. A. Rosati. An immersed boundary method for complex incompressible flows. *J. Comput. Phys.*, 224:757-784, 2007.
- [4] C. Liu and C. Hu. An efficient immersed boundary treatment for complex moving object. *J. Comput. Phys.*, 274:654-680, 2014.
- [5] Y. T. Ng, C. Min, and F. Gibou. An efficient fluid-solid algorithm for single-phase flows. *J. Comput. Phys.*, 228:8807-8829, 2009
- [6] K. Yokoi, Efficient implementation of THINC scheme: A simple and practical smoothed VOF algorithm. *J. Comput. Phys.*, 226:1985-2002, 2007.
- [7] D.L. Youngs. Time-dependent multi-material flow with large fluid distortion. In: K.W. Morton, M.J. Baines (Eds.), *Numerical Methods for Fluid Dynamics*, 24: 273-285, 1982.
- [8] H. T. Ahn and M. Shashkov. Adaptive moment-of-fluid method. *J. Comput. Phys.*, 228:2792-2821, 2009.
- [9] A. Chorin. A numerical method for solving incompressible viscous flow problem. *J. Comput. Phys.*, 2: 12-26, 1967.
- [10] F. Gibou, R. Fedkiw, L.-T. Cheng, and M. Kang. A second-order-accurate symmetric discretization of the Poisson equation on irregular domains. *J. Comput. Phys.*, 176: 205-227, 2002.
- [11] C. W. Hirt and B.D. Nichols. Volume of fluid (VOF) methods for the dynamic of free boundaries. *J. Comput. Phys.*, 39:201-225.
- [12] M. Braza, P. Chassaing, and H. H. Minh. Numerical study and physical analysis of the pressure and velocity fields in the near wake of a circular cylinder, *J. Fluid Mech.*, 165:79-130, 1986.
- [13] C. Liu, X. Sheng, and C.H. Sung, Preconditioned multigrid methods for unsteady incompressible flows, *J. Comput. Phys.*, 139: 35-57, 1998.
- [14] C. Norberg. Flow around a circular cylinder: Aspects of fluctuating lift. *J. Fluid Struct.*, 15:459-469, 2001.
- [15] C.H.K. Williamson. Oblique and parallel models of vortex shedding in the wake of a circular cylinder at low Reynolds numbers. *J. Fluid Mech.*, 206: 579-627, 1989.
- [16] H. Wang, J. Chessa, W.K. Liu, and T. Belytschko. The immersed/fictitious element method for fluid-structure interaction: volumetric consistency, compressibility and thin members. *Int. J. Numer. Methods Eng.*, 74: 32-55, 2008.
- [17] J. C. Martin and W. J. Moyce. An experimental study of the collapse of liquid columns on a Rigid horizontal plane. *Philosophical transactions of the royal society of London, series A, mathematical and physical sciences*, 244:312-324, 1952.